ARTICLES

Electronic Properties of Neutral Dyes in the Channels of Zeolite L: A Combined Spectroscopic and Quantum Chemical Study

Beate Bussemer,* Dirk Munsel, Heike Wünscher, Gerhard J. Mohr, and Ulrich-Walter Grummt

Institute of Physical Chemistry, Friedrich-Schiller University Jena, Lessing St. 10, D-07743 Jena, Germany

Received: August 3, 2006; In Final Form: October 13, 2006

Three low molecular weight model compounds for poly(phenylene−ethynylene)s were inserted into the channels of zeolite L by using gas phase insertion. The absorption and emission spectra in solution and dye/zeolite L are reported. Two compounds show emission properties in zeolite L comparable to that in solution. In contrast, the bipyridine containing compound shows a red shift toward longer excitation wavelengths. Matrix rank analysis of the emission spectra gave three contributing species. Quantum chemical calculations provide different conformations depending on the Si/Al distribution of the framework and the extraframework cations and attached protons.

Introduction

Conjugated polymers have recently gained particular interest mainly, but not exclusively, because of their successful applications as organic light emitting diodes and due to the possibility to produce cheap and flexible photovoltaic elements.[1−8] Designing optimized materials for these applications and designing the devices themselves requires a profound knowledge of their spectroscopic and photophysical properties. A key issue for understanding and predicting not only the details of radiative transitions but also of nonradiative transitions is the coupling of the electron and nuclear motion, which can be derived from the Franck−Condon integrals for the initial and final states.[9] Evaluation of Franck−Condon overlap integrals, in turn, requires knowledge of vibrationally well-resolved electronic transitions.

It is common to many conjugated polymers that their longest wavelength electronic absorption band does not show vibrational resolution, at least at ambient temperature, whereas their emission spectra frequently exhibit poorly resolved spectra. This behavior is explained by a more rigid structure of the excited state according to the rules of Imamura and Hoffmann.[10] When decreasing the temperature, often vibrationally resolved absorbance spectra are observed due to freezing of torsional motions of the ground state molecule, see for example Grummt et al.[11] However, in order to perform a detailed Franck−Condon analysis a much better resolution is required.

The conjugation length of poly(phenylene−ethynylene)s and their analogue heterocyclic polymers is comparatively small, roughly 2−3 repetition units.[11] Therefore, low molecular weight model compounds represent, nearly perfectly, the photophysics of the polymer in diluted solution (with the exception of energy migration effects along the backbone). Hence, we confine our interest on model compounds.

* Corresponding author phone: +49 3641 948352; fax: +49 3641 948302; e-mail: beate.bussemer@uni-jena.de.

Among the most versatile techniques to obtain highly resolved excitation or emission spectra is luminescence spectroscopy of supersonic molecular jets. Unfortunately all our attempts to record luminescence from molecular jets with low molecular weight model compounds failed.[12]

Another possibility to obtain quasi line spectra is offered by the Shpol'skii effect.[13] However Shpol'skii matrices are limited in that often thermodynamic nonequilibrium states are involved, rendering the spectroscopic results dependent on concentration and cooling conditions. Because our compounds tend to aggregate already in highly diluted solution upon lowering the temperature, Shpol'skii spectroscopy does not appear to be promising.

Therefore, we decided to use inclusion compounds in order to prevent aggregation effects and to allow a sufficient degree of motional freedom to allow thermal equilibration at low temperature.

Usage of L-zeolites as hosts for otherwise strongly aggregating dyes has been pioneered by Calzaferri et al.[14−16] Zeolite L is a microporous material with a one-dimensional tube structure. Zeolite L crystals are of hexagonal symmetry (P6/*mmm*).[17] Their unit cell forms a rhomb at the bottom and thus the primitive vectors $\boldsymbol{a}$ and $\boldsymbol{b}$ have the same length (1.84 nm). They form angles of 60° and 120° respectively. The vector $\boldsymbol{c}$ (0.75 nm) is perpendicular to $\boldsymbol{a}$ and $\boldsymbol{b}$ and is parallel to the central axis of the zeolite crystals. The main channels run parallel along that axis straight through the crystals. The Si:Al ratio is 3:1, where Si and Al atoms are statistically distributed in the framework. Each channel can be filled with dye molecules. In the ideal case, no interaction should occur between inserted molecules.

The chemical, photochemical, and photophysical properties of inserted molecules are largely influenced by the geometrical constraints imposed by the host. The electronic spectra are well-known to be sensitive to the molecular conformation and to

10.1021/jp064986w CCC: $37.00
Published on Web 12/15/2006

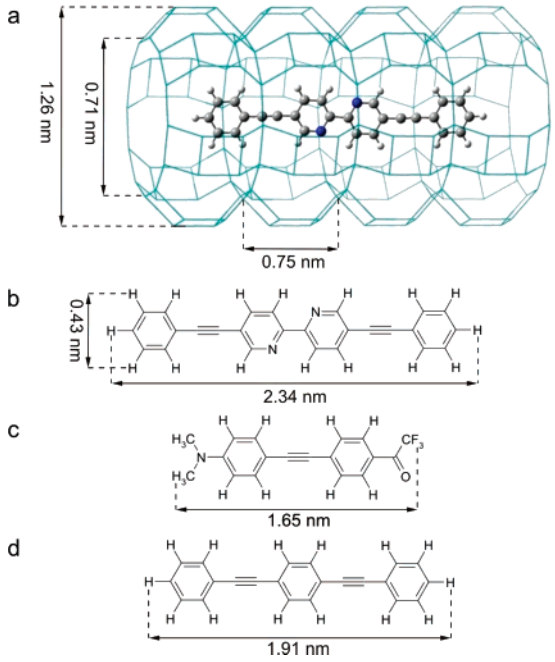

Figure 1. (a) One possible orientation of **Bpy2** in a channel of zeolite L. The free pore diameter is 0.71 nm. The channel diameters and molecular dimensions are based on van der Waals radii. The length of a unit cell is 0.75 nm. (b) structure and dimension of **Bpy2** (c) structure and dimension of **Tol2 (**d) structure and dimension of **BPB**.

the chemical environment of the sorbate. They also depend on the presence of solvent molecules, as coadsorbed water, and co-cations.

The purpose of this paper is to investigate the influence of the zeolite framework on the spectroscopic properties of *5,5′-di(phenylethynylene)-2,2′-bipyridine* (**Bpy2**). The effect of the distribution of the Si and Al atoms, the interaction with extraframework cations of the host, the interaction with solvent molecules, as well as the sorbate loading are examined.

Figure 1a shows the structure and one of the possible orientations of **Bpy2** inside a zeolite pore.

Furthermore, for comparison, we choose *1-[4-(4-dimethylamino-phenylethynyl)-phenyl]-2,2,2-trifluoro-ethanone* (**Tol2**) and *tri(phenylethynylene)* (**BPB**) for our study, the structures of which are shown in Figure 1b−d. Their molecular dimensions are favorable for insertion into the zeolite, and they also contain a phenylene−ethynylene-unit, but no bipyridine moiety. We want to compare the fluorescence behavior of these molecules inside the zeolite.

Experimental Methods

Synthesis. All educts were purchased from Fluka or Aldrich.

Information on synthetic procedures of *5,5′-di(phenylethynylene)-2,2′-bipyridine* (**Bpy2**) and *tri(phenylethynylene)* (**BPB**) can be found at Egbe et al.[18] and Nakatsuji et al.,[19] respectively.

1-[4-(4-dimethylamino−phenylethynyl)-phenyl]-2,2,2-trifluoro−ethanone (**Tol2**):

A mixture of 0.5 g of 1-ethynyl-4-*N*, *N*-dimethylaniline, 0.8 g of 4′-bromo-2,2,2-trifluoroacetophenone, 50 mg of copper-(I)iodide, 30 mg of palladium diacetate, 75 mg of tri-o-tolylphosphine and 4 mL of triethylamine were heated at 80 °C for 6 h in a capped heavy-wall pyrex tube that was flushed with dry nitrogen. To the cooled solution water was added and 50 mL of dichloromethane and the aqueous layer extracted two times with 50 mL of dichloromethane. The combined dichloromethane solutions were washed three times with distilled water, dried over magnesium sulfate and evaporated to dryness. Purification by flash chromatography on silica gel 60 using a mixture of hexane/dichloromethane (1:1 = v/v) as the eluent gave 0.7 g of *1-[4-(4-dimethylamino-phenylethynyl)-phenyl]-2,2,2-trifluoro−ethanone* (**Tol2**) as fine yellow-orange crystals, mp = 173−175 °C.

^{1}H−NMR ($CDCl_3$) δ (ppm): 8.02 (d, 2 H, =CH-), 7.61 (d, 2 H, =CH-), 7.44 (d, 2 H, =CH-), 6.67 (d, 2 H, =CH-), 3.02 (t, 6 H, -CH_3).

MS (DEI) m/e: 317 [M], 248 [M− CF_3], 220 [M− $COCF_3$].

Calculated for $C_{18}H_{14}F_3NO$ (%): C, 68.13; H, 4.45; N, 4.41; found: C, 68.46; H, 4.59; N, 4.18.

The absorption and emission spectra of **Tol2** in chloroform are presented in Figure 2.

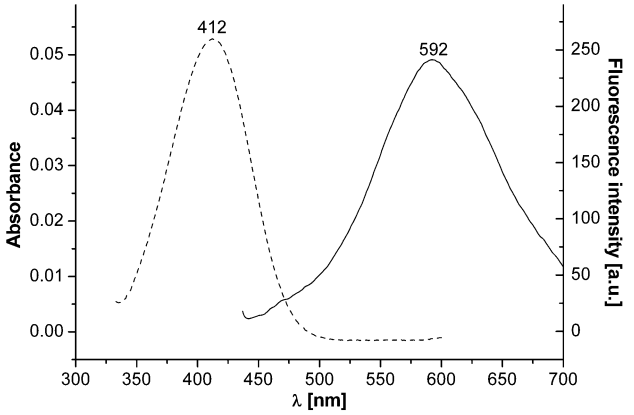

Figure 2. Absorption (dashed line) and corrected emission spectra (solid line) of **Tol2** in chloroform.

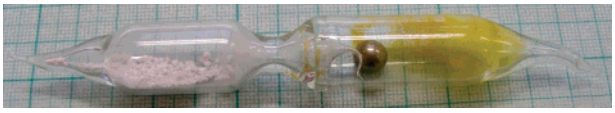

Figure 3. Image of the ampule needed for the insertion from the gas phase.

Zeolite L. The synthesis of the pure potassium form of zeolite L crystals ($K_9(AlO_2)_9(SiO_2)_{27}\cdot 21H_2O$) was carried out according to the standard procedure under static conditions.[15]

Synthesis of Dye/Zeolite L Composites. For neutral dyes the gas phase insertion into the zeolite is most appropriate. This procedure was performed with the double ampule method[16] under slightly modified conditions. First, the zeolite crystals were dehydrated. They were filled in one side of a glass ampule (see Figure 3) and then heated to 620 K at a pressure of 5×10^{-1} Pa. After 12 h of heating, the ampule was sealed. The second half of the ampule was then filled with the neutral dye and dried at a temperature below its melting point. After 2 h the ampule was sealed, and the hook, which separates the ampule sites, was broken by the steel ball. The insertion of the dye into the zeolite was performed by sublimation between 5 and 10 h.

The insertion was followed by the washing procedure of loaded zeolite crystals to eliminate dye molecules adsorbed on the outer surface of the crystals. Chloroform (spectroscopic grade) was added to the dry zeolite L sample. Then the mixture was homogenized mechanically before it was put into a centrifuge Hermle Z 320 for 5 min at approximately 4200 revolutions/minute. The rinsing solution was separated and used to record an absorption spectrum. The procedure was repeated until the absorption of the dye in the solvent was negligible. At that point the remaining dye is assumed to be located exclusively inside the channels of zeolite L.

Characterization of Zeolite L. The porosity of the zeolite L crystals was established by an aqueous thionine acetate solution.[14]

The actual shape of the synthesized zeolite L crystals was checked with a Zeiss DSM 940 A scanning electron microscope (SEM).

X-ray Diffraction. The structure of the zeolite was examined by X-ray powder diffraction with a Freiberger Präzisionsmechanik URD 6 diffractometer equipped with a Bragg−Brentano setup using Mo−K_α radiation (60 kV, 50 mA) in the 2θ range from 1 to 60°. To evaluate and refine the powder pattern we used the software Powder Cell 2.4.

Determination of the Pore Volume Before and After Loading. Nitrogen adsorption and desorption isotherms were recorded using an Autosorb-1 (Quantachrome) at 77 K. 160 mg of zeolite were dehydrated at 620 K for 12 h at 5×10^{-1} Pa. From these isotherms the specific surface area and the pore volume of the zeolite L crystals were determined. The multipoint BET method (p/p_0: 0.054−0.298)[20,21] and the Langmuir method (p/p_0: 0.054−0.895) were used for the determination of the specific surface area. The calculation of the pore volume of the crystals refer to 77.35 K at the relative pressure p/p_0 of 0.978.

Theoretical Approach Toward the Dye Loading of Zeolite L. To determine the theoretical mass of dye (m_d) needed for a 100% load of the zeolite L crystals we assume that the length of all channels (l_{ch}) are completely occupied by dye molecules with the length l_d and the molar weight M_d. Hence we get this equation:

$$m_d = \frac{l_{ch} \cdot M_d}{N_A \cdot l_d} \tag{1}$$

The total length of all channels can be determined according to Calzaferri et al.[18] with the following equation:

$$l_{ch} = \frac{m_z}{\rho_z \cdot |a^2| \cdot \sin 60°} = 1.57 \times 10^{13}\ \text{cm} \tag{2}$$

where m_z is the mass of the used zeolite, ρ_z is its density, and a is the length of the unit cell (0.75 nm).

With the length of one **Bpy2** molecule ($l_d = 0.43 \times 10^{-7}$ cm), and the calculated total pore length of 1 g zeolite L, the total number of dyes N_d incorporated in the pores at 100% loading can be calculated as follows:

$$N_d = \frac{l_{ch}}{l_d} = 6.17 \times 10^{16} \tag{3}$$

The total volume of all incorporated **Bpy2** molecules for a 100% loading is then

$$V_d = N_d \cdot v_d = 0.0114\ \text{cm}^3 \tag{4}$$

where v_d is the volume of one dye molecule ($v_d = 0.171 \times 10^{-21}$ cm^3).

Finally, the effective loading level can be determined:

$$\frac{V_{ch}^p - V_d}{V_{ch}^l} \tag{5}$$

where V_{ch}^p is the pore volume of the pure zeolite L and V_{ch}^l is the pore volume of the dye loaded zeolite L.

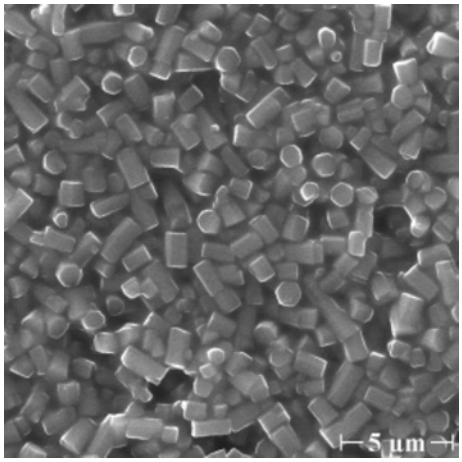

Figure 4. SEM image of the synthesized zeolite L crystals.

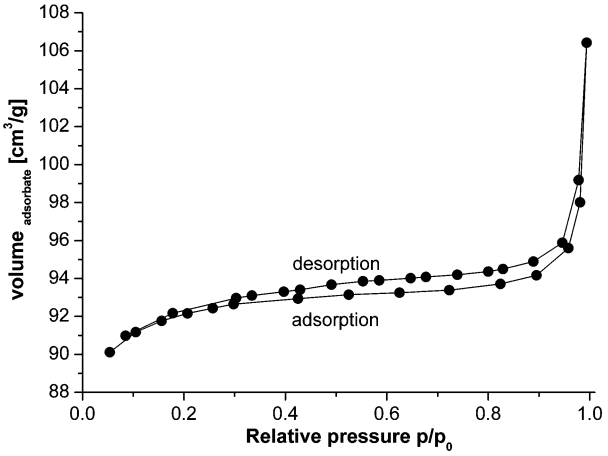

Figure 5. Adsorption and desorption isotherms of the synthesized zeolite L crystallites.

Spectroscopy. Absorption spectra were recorded by a Varian Cary 5000 spectrometer using quartz cuvettes.

Fluorescence spectra were recorded with a Spex Fluorolog-3 fluorometer. For the fluorescence measurements of the loaded zeolite L crystals thin layers on quartz discs were prepared.

All spectra were recorded at room temperature.

Results and Discussion

Zeolite L. The SEM image of the synthesized crystallites (Figure 4) reveals the typical hexagonal structure of the crystals. An average size of the produced crystals was determined with a length of 1.7 μm and a diameter of 0.9 μm. The powder pattern obtained by X-ray diffraction reveals a zeolite L structure which is in good agreement to previously synthesized zeolite L crystals.[22−24]

The measured isotherm (see Figure 5) corresponds to a Langmuir isotherm and is typical for microporous solids with relatively small external surfaces such as zeolites. The specific surface area calculated with the multipoint BET method results in 276.3 m^2/g, whereas the Langmuir method gave 410.0 m^2/g. The pore volume of the pure zeolite L V_{ch}^p was determined as 0.153 cm^3/g.

For the **Bpy2** loaded zeolite L the specific surface area calculated with the BET method was 224.1 m^2/g, the Langmuir method gave 340.3 m^2/g. The pore volume V_{ch}^l of the dye loaded zeolite L is 0.142 cm^3/g.

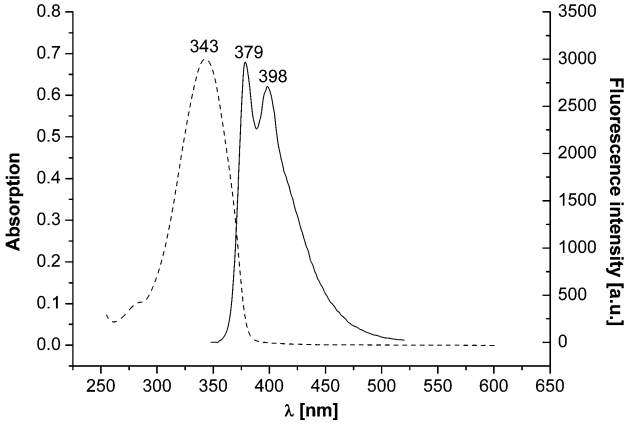

Figure 6. Absorption spectrum of **Bpy2** in chloroform.

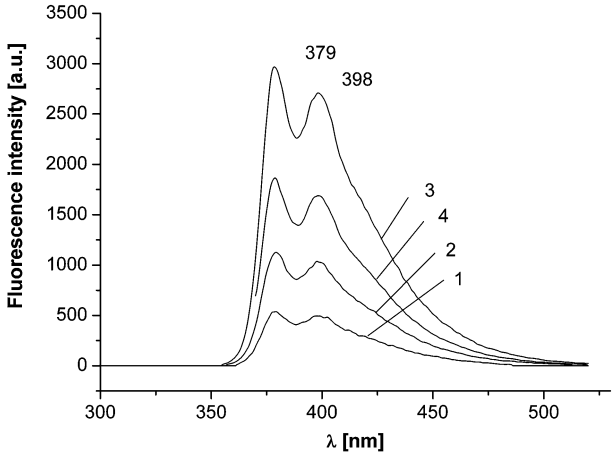

Figure 7. Series of corrected emission spectra of **Bpy2** in chloroform. Excitation wavelengths: (1) 268 nm, (2) 309 nm, (3) 343 nm, and (4) 365 nm.

From the values for the pore volumes we determined the effective loading level of **Bpy2** in zeolite L using eq 5.

$$\frac{V_{\mathrm{ch}}^{p} - V_{\mathrm{d}}}{V_{\mathrm{ch}}^{l}} = 99.6\%$$

Note that the load estimation assumes that the N_2 molecules can occupy all the internal volume not occupied by the adsorbed organic molecule. Because of pore blocking by the dye and because of packing requirements of N_2 itself, the obtained value is the upper limit of the possible dye loading estimated from the pore volumes before and after loading.

Absorption and Fluorescence Spectroscopy. Bpy2 exhibits an unstructured absorption band with a maximum at 343 nm in chloroform as illustrated in Figure 6.

The emission spectrum shows a vibrational structure and is independent of the excitation wavelength (Figure 7).

The dye inserted into the zeolite L, however, shows anomalous fluorescence (see Figure 8).

The vibrational structure is completely lost. In addition, a systematic red shift was observed with increasing excitation wavelengths. A total shift of 63 nm between the shortest (309 nm) and the longest (442 nm) excitation wavelength was observed.

To exclude the effect of reabsorption, we investigated another series of emission spectra with a dye loading of 20% (Figure 9). It shows the same behavior as in the case of 99.6% dye loading. Hence we can definitely rule out reabsorption as a reason of the spectral shift and attribute the latter to the existence of different species or sites.

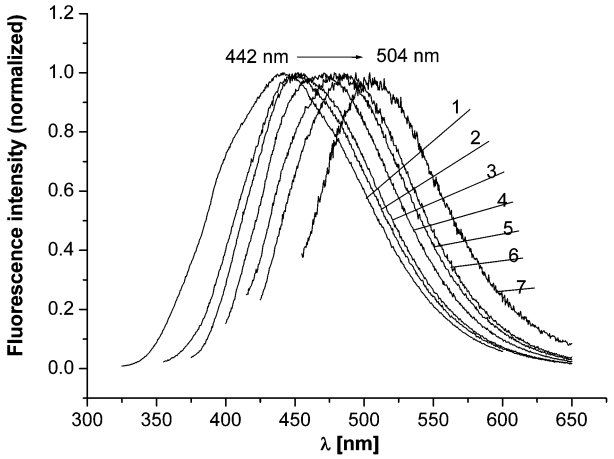

Figure 8. Series of corrected emission spectra of **Bpy2** incorporated in zeolite L crystals with a dye loading of 99.6%. Excitation wavelengths: (1) 309 nm, (2) 343 nm, (3) 365 nm, (4) 390 nm, (5) 402 nm, (6) 412 nm, and (7) 442 nm. Red shift: 62 nm.

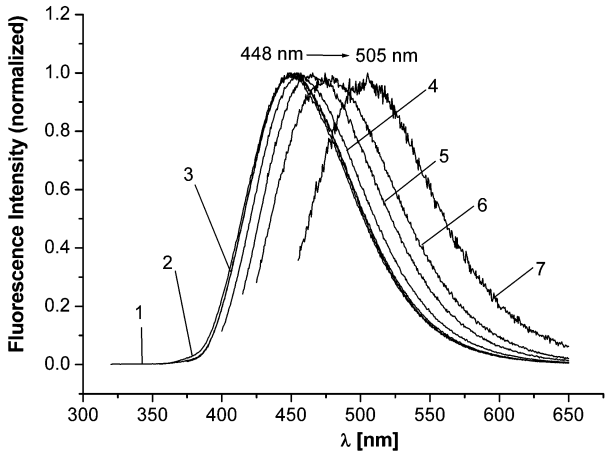

Figure 9. Series of corrected emission spectra of **Bpy2** incorporated in zeolite L crystals with a dye loading of 20%. Excitation wavelengths: (1) 309 nm, (2) 343 nm, (3) 365 nm, (4) 390 nm, (5) 402 nm, (6) 412 nm, and (7) 442 nm. Red shift: 63 nm.

In contrast to **Bpy2,** both **Tol2** and **BPB** incorporated in zeolite L crystals do not exhibit anomalous fluorescence behavior. Neither a blue shift nor a red shift of the emission spectra of the zeolite samples was observed. A measured series of emission spectra reveals only variations within the limits of error. This is demonstrated in Figures 10 and 11.

To obtain the number of species that exhibit independent fluorescence emission, all fluorescence spectra of **Bpy2** were evaluated by matrix rank analysis.[25] For all series of spectra we obtained three independent components, where the third component shows an significantly smaller contribution.

Quantum Chemical Calculations. The current quantum chemical calculations have been performed in order to evaluate the factors that influence the fluorescence emission spectrum of **Bpy2** in zeolite L. Possible factors can be the distribution of the Si and Al atoms in the zeolite L framework, the interaction of the dye molecule with coadsorbed water, interaction with the co-cations at the positions near to the channel walls, or interaction with adsorbed protons along the channels, which can form Si−OH−Al groups and thus act as Brønstedt acids.

All calculations were performed using Gaussian 03.[26]

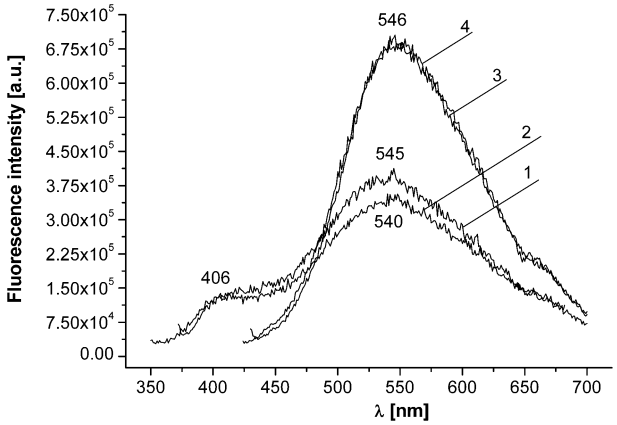

Figure 10. Series of corrected emission spectra of **Tol2** incorporated in zeolite L crystals. Excitation wavelengths: (1) 365 nm, (2) 398 nm, (3) 412 nm, and (4) 422 nm.

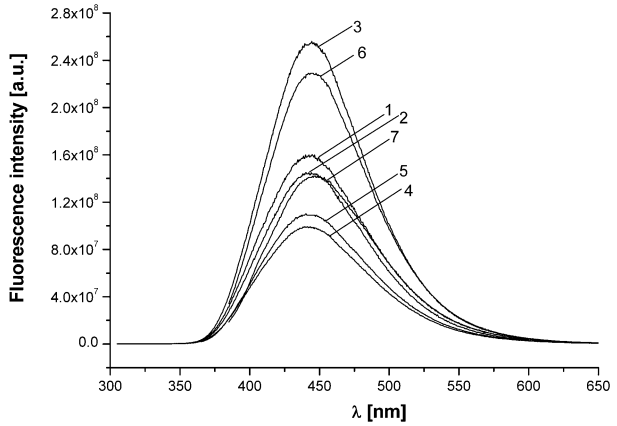

Figure 11. Series of emission spectra of **BPB** incorporated in zeolite L crystals. Excitation wavelengths: (1) 290 nm, (2) 314 nm, (3) 322 nm, (4) 342 nm, (5) 355 nm, (6) 363 nm, and (7) 375 nm.

Bpy2, in contrast to **Tol2** and **BPB**, contains a 2,2′-bipyridine unit whose structure and conformation have been the subject of numerous experimental and quantum chemical investigations. The crystal structure of 2,2′-bipyridine determined by X-ray diffraction is coplanar with a *trans* conformation.[27] In aqueous and organic solvents the same conformer is found, whereas in acidic solution the *cisoid* conformer is preferred.[28] Quantum chemical investigations of the rotational barrier with several model chemistries and basis sets confirm the *transoid* coplanar structure for the electrically neutral molecule and a *cisoid* structure for a single protonated molecule.[29,30]

Investigations on 2,2′-bipyridine in nonacidic MFI zeolites show a stabilization of a *cisoid* conformation through the cation-N contacts.[31]

The same factors which can influence the conformation of 2,2′-bipyridine in neutral or acid solution are assumed to be responsible for different **Bpy2** conformers in zeolite L.

While the preparation of the dye/zeolite composites was performed in high vacuum, the spectroscopic measurements were carried out under ambient conditions. Consequently, water can be readsorbed into the channels and protons can be formed upon its interaction with the Si−O−Al sites.

To investigate the influence of coadsorbed water, protons as well as potassium ions on the conformation of **Bpy2**, we optimized the structures of the S_0 and the S_1 state of the *transoid* and the *cisoid* conformer of **Bpy2** as isolated molecule, and together with one water molecule, one proton, or one potassium ion, respectively.

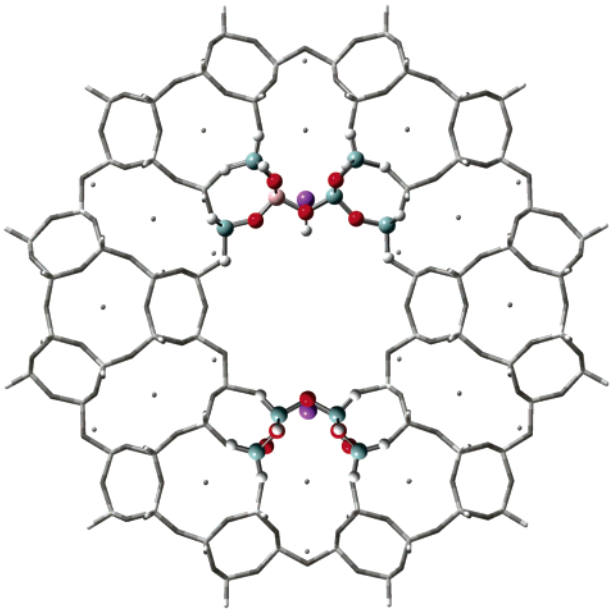

Figure 12. Parts of zeolite L framework with K^+ and H^+, respectively, used for cluster calculations of **Bpy2**.

As a next step, we investigated the interaction of the **Bpy2** molecule with the zeolite framework containing a proton or a K^+ ion. We performed structure optimizations of **Bpy2** interacting with two different clusters, which were cut out from the zeolite framework (see Figure 12). The acidic cluster consists of nine tetrahedra (7 Si, 2 Al) and contains one H^+ ion and one K^+ ion. The second cluster is constructed from 8 tetrahedra (7 Si, 1 Al) and contains one K^+ ion. The dangling bonds were saturated with hydrogen atoms. During the optimization all atoms were allowed to relax except the saturating H-atoms.

The structures for the S_0 and the S_1 state of all species were optimized and the absorption and emission maxima were calculated. For the S_1 state structure optimization and the calculation of the emission maxima the CI singles method was applied. This method is a time- and resource-consuming procedure; therefore, the moderate basis set 6-31g(d) was used during the calculations (CIS/6-31g(d)).

Since the accuracy of the CI singles calculations for an excited state corresponds to that of a HF calculation for a ground state, the Hartree−Fock approach was applied together with the same basis set for the optimization of the S_0 states (HF/6-31g(d)). The absorption wavelength for the optimized structure was calculated with the CI singles method and the same basis set (CIS/6-31g(d)). With this combination of methods an internal consistency of the results and an exact caracterization of the chemical behavior is guaranteed and a direct comparison of the calculated structures, energies and absorption and emission wavelengths on the same level of theory is possible.

Table 1 shows the results of all calculations (absolute energies, energy difference between *transoid* and *cisoid* conformer, absorption and emission maxima).

*Interaction of **Bpy2** with H_2O, H^+, or K^+.* The *transoid* and *cisoid* conformers of the isolated **Bpy2** molecule have planar structures in both S_0 and S_1 state (Figure 13a). The energy difference between *cisoid* and *transoid* is about 30 kJ/mol, where the *transoid* conformer is in both cases the more stable one. The *transoid* and the *cisoid* form have almost the same excitation and emission maximum. Hence they may not be distinguishable in the absorption and the fluorescence spectra.

The addition of one water molecule does not affect the planar **Bpy2** structures and the energy difference between the *transoid*

TABLE 1: Ground State Energies, Excited-state Energies, Absorption, and Emission Wavelengths of Bpy2 with Different Added Species and with Part of Zeolite L Framework

		transoid conformer		*cisoid* conformer		ΔE ($E_{cisoid} - E_{transoid}$)/
		energy/a.u.	λ/nm	energy/a.u.	λ/nm	kJ/mol
Bpy2	S_0 state	−1102.72	271	−1102.71	270	34.63
	S_1 state	−1102.71	322	−1102.69	320	34.72
Bpy2+ H_2O	S_0 state	−1178.74	272	−1178.73	272	30.64
	S_1 state	−1178.72	323	−1178.71	323	23.81
Bpy2+ H^+	S_0 state	−1103.10	306	−1103.11	304	−29.57
	S_1 state	−1103.09	367	−1103.10	365	−28.82
Bpy2+ K^+	S_0 state	−1701.73	268	−1701.74	281	−36.34
	S_1 state	−1701.71	337	−1701.73	336	−43.34
Bpy2 + part of zeolite L + H^+	S_0 state	−4454.92	273	−4454.91	257	11.34
	S_1 state	−4454.91	327	−4454.90	325	19.36
Bpy2 + part of zeolite L + K^+	S_0 state	−4575.26	277	−4575.25	261	26.25
	S_1 state	−4575.23	327	−4575.23	325	10.41

and the *cisoid* conformer (Figure 13b). Again, the *transoid* conformer is more stable in S_0 as well as in S_1 state. Moreover, the excitation and the emission wavelengths are not influenced by the addition of water, as the difference to the isolated molecule is only about 2 nm.

When optimizing the structure with an added proton, a planar *cisoid* conformer of **Bpy2** becomes more stable in S_0 and in S_1 state (Figure 13c). Furthermore the absorption and the emission wavelengths are influenced by the proton and shifted to longer wavelengths. In the S_0 state there is a shift of about 35 nm from the electrically neutral molecule to the protonated one, in the S_1 state the shift increases to 45 nm. Even when protonated, the *cisoid* and the *transoid* conformer are planar with similar absorption and emission maxima.

After adding a K^+ cation to **Bpy2**, the *cisoid* conformer is more stable in S_0 and S_1 state. In S_0 state the *transoid* form is deplanarized while the *cisoid* form is planar (Figure 13d). This is probably the reason for the long wavelength shift in the absorption maximum of the *cisoid* form.

In the S_1 state, both conformers are planar and thus show the same emission maximum (Figure 13e). The energy differences between the *cisoid* and the *transoid* conformer in ground state and in excited state is 60 and 67 kJ/mol, respectively.

*Interaction of **Bpy2** with a Selected Entity of the Zeolite L Framework.* When optimizing **Bpy2** with the zeolite cluster containing H^+, the *cisoid* conformer of **Bpy2** becomes nonplanar in S_0 state, and hence the absorption maximum is at a shorter wavelength compared to the *transoid* conformer (difference 16 nm, Figure 14a), but in S_1 state both conformers are planar with almost the same emission maximum (difference 2 nm, Figure 14b). Unlike a single proton interacting with **Bpy2** and forming a **[Bpy2H]**$^+$ ion, a proton bound to the zeolite neither stabilizes the *cisoid* conformer of **Bpy2** in S_0 and S_1 state nor protonates the **Bpy2** molecule, it only lowers the energy difference between the conformers.

The interaction of **Bpy2** with the K^+ ion of zeolite L results in almost the same properties as the interaction with the zeolite cluster containing H^+. In S_0 state, the *cisoid* conformer is nonplanar and shows an absorption maximum shifted to a shorter wavelength in comparison to the *transoid* conformer (difference 16 nm, Figure 15a), while in S_1 state, both conformers are planar

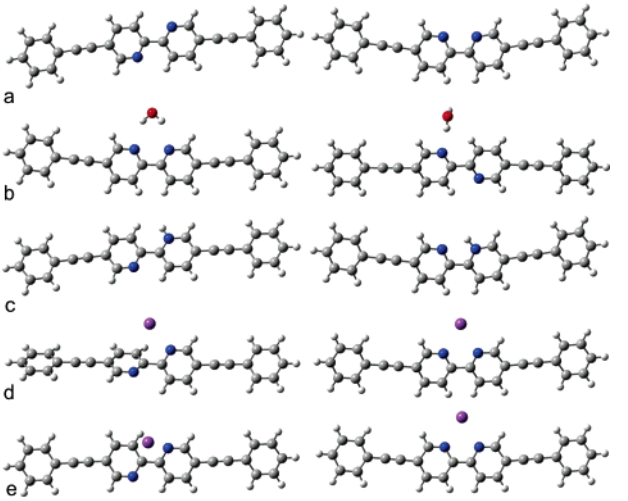

Figure 13. Optimized structures of the *transoid* and the *cisoid* conformer of **Bpy2** (a) **Bpy2**, isolated molecule, S_0 state (b) **Bpy2** with H_2O, S_0 state (c) **Bpy2** with H^+ ion, S_0 state (d) **Bpy2** with K^+ ion, S_0 state (e) **Bpy2** with K^+ ion, S_1 state.

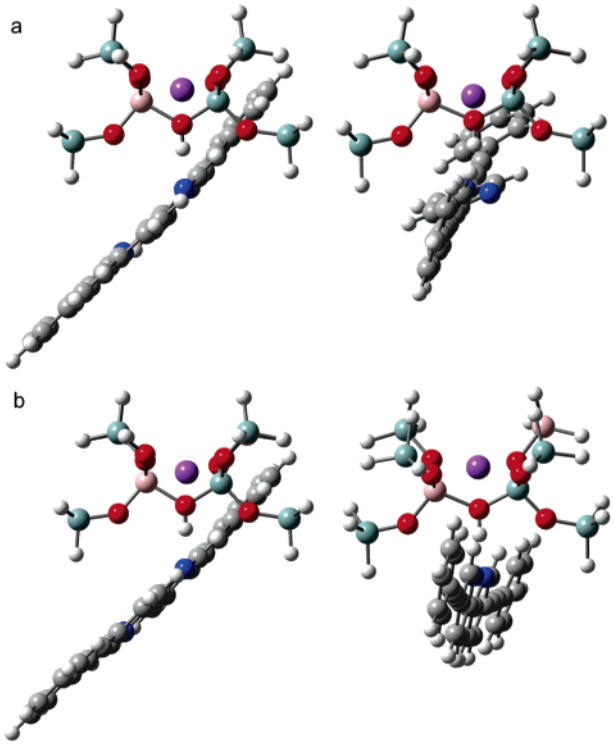

Figure 14. Optimized structure of the *transoid* and the *cisoid* conformer of **Bpy2** with H^+ and a part of zeolite L pore (a) ground state structure (b) excited-state structure.

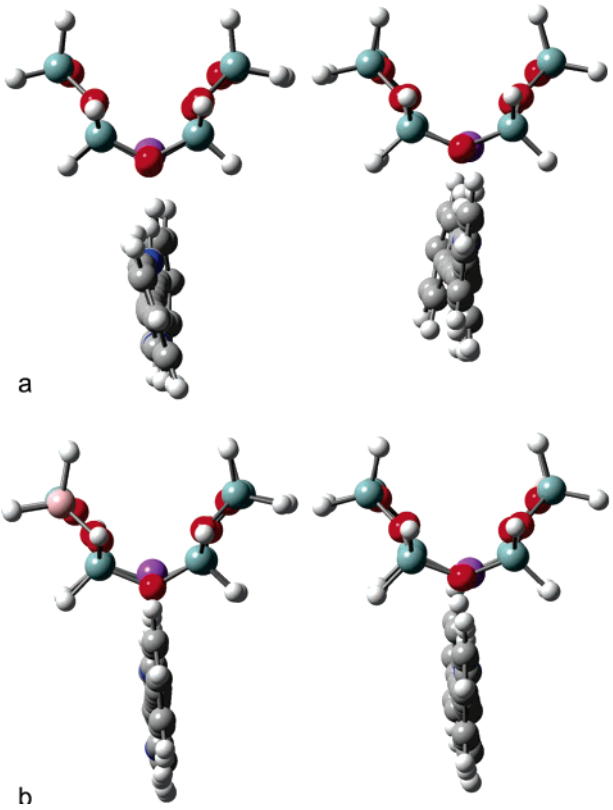

Figure 15. Optimized structures of the *transoid* and the *cisoid* conformer of **Bpy2** with K^+ and a part of zeolite L pore (a) ground state structure (b) excited-state structure.

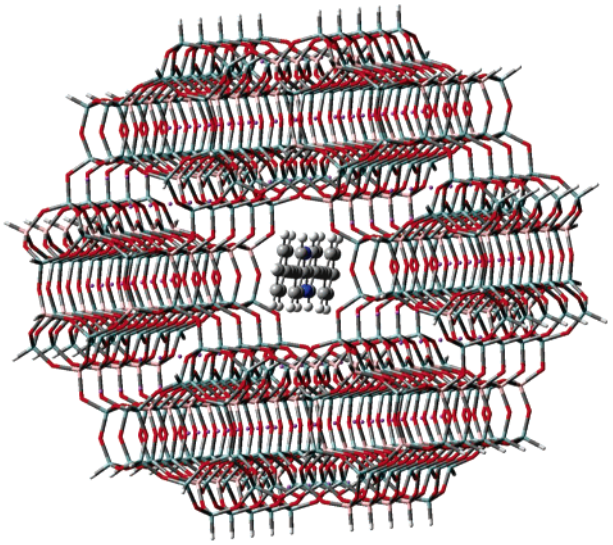

Figure 16. Part of zeolite L framework used for ONIOM calculations, with inserted **Bpy2** molecule.

with an emission maximum difference of 2 nm (Figure 15b). Again, the cation bound to zeolite L does not stabilize the *cisoid* conformer.

Si/Al Distribution. To investigate the influence of the statistical Si/Al distribution on the absorption and emission spectra of **Bpy2**, we used the ONIOM approach[32−34] of the Gaussian program package since the dye molecule can be treated at a high level of theory, whereas the zeolite part can be considered at a much lower level.

In our calculations the zeolite part was represented by a cylindrical cluster around a pore (see Figure 16). The dangling bonds were saturated with H atoms in order to keep the whole

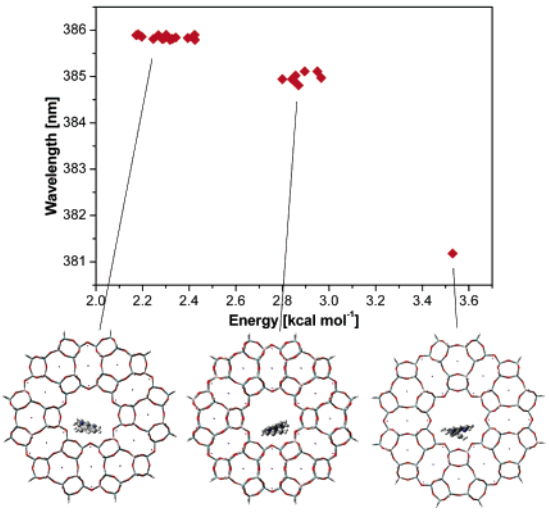

Figure 17. Ground state energy of **Bpy2** relative to absorption wavelength.

system neutral. The number of Si and Al atoms were 408 and 132, respectively. With this system, 26 Si/Al distributions were generated randomly. To fulfill Löwenstein's rule, no neighbored Al atoms were created.

The system was treated with the two-layer ONIOM approach. The outer layer consists of the zeolite L part and is treated with the Universal Force Field (UFF). Its structure was fixed during the calculation. The inner layer is the **Bpy2** molecule. We focused on its S_0 state, because, on our computers, it was not possible to use the CI singles method together with the ONIOM approach. Since we do not directly compare the results from the cluster calculations with that of the ONIOM calculations, we applied density functional methods to the high layer. The **Bpy2** structure was optimized with the B3LYP functional, the basis set was 6-31g(d). After optimization, an excited-state energy calculation with the time-dependent DFT method (TD-B3LYP/6-31g(d)) was performed to obtain the excitation energies of **Bpy2**. To have the high layer system solved in the field created by partial charges of the mechanics atoms we used the "EmbedCharge" option of the ONIOM approach.

The upper part of Figure 17 presents the absorption wavelength of **Bpy2** in zeolite L as a function of the ground state energy of **Bpy2** in the pore. The energy is the difference to the ground state energy of the isolated optimized molecule (B3LYP/6-31g(d)). Three distinct energy regions are formed where the third energy region has only one member.

The lower part of Figure 17 shows three characteristic optimized structures for each of the energy regions. The region with the lowest energy is connected with the longest absorption wavelength and with the most planar structure, while the region with the highest energy is connected with the shortest absorption wavelength and with the most deplanarized **Bpy2** structure. The different Si/Al distributions cause different deviations from the planar structure and hence different absorption maxima. Although not explicitly calculated, the same should be true for the emission maxima of **Bpy2**.

The difference in the calculated absorption maxima is 5 nm. The comparison between this difference and the experimental red shift of 63 nm in the emission spectra reveals that the Si/Al distribution contributes to the shift of the emission wavelength.

Though this result may not quantitatively explain the strong shift in the emission maximum, it is in accordance with the matrix rank analysis where also three different species were

found. We conclude that, inside the channels, three conformers contribute to the various emission spectra.

Conclusions

The present spectroscopic experiments support the notion that **Bpy2** is sorbed as an intact molecule in dehydrated zeolite L. Zeolite L influences the emission spectra of **Bpy2** (loss of vibrational structure, red shift) but not of **Tol2** and **BPB**. Conceivably this is due to the statistical Si/Al distribution in the zeolite L framework, while interactions between the N atoms of the 2,2′-bipyridine unit and extra framework K^+ cations or with the protons formed by water readsorption are of no major importance. Matrix rank analysis of the spectra yield three spectroscopically active species in case of **Bpy2**. The inclusion of **Bpy2** in the channels of zeolite L is obviously an inappropriate method to obtain vibrationally resolved emission spectra.

The quantum chemical investigations using HF(6-31g(d)), CIS(6-31g(d)), ONIOM(B3LYP/6-31g(d):UFF), ONIOM(TD-B3LYP/6-31g(d):UFF) provide a structural support to the interpretation of spectroscopic results in the following:

(1) coadsorbed water does not influence the emission wavelength;

(2) while the interactions of an isolated **Bpy2** molecule with H^+ or K^+ stabilizes its *cisoid* conformation, the protonated zeolite L channel and the extra framework K^+ ion near the channel walls yield a *transoid* conformation both for S_0 and S_1 state;

(3) the emission maximum of the occluded **Bpy2** is not influenced by the zeolite framework as the difference to the emission of the isolated molecule is only 2 nm both in ground and in excited state for all conformers;

(4) the *trans*- and the *cis*-planar conformation of **Bpy2** have the same emission maximum due to their equal chromophore size;

(5) only the Si/Al distribution contributes to changes of the **Bpy2** geometries and hence to changes in the emission maxima.

Our results show that differences in the absorption and the emission maxima are only possible when the **Bpy2** structure is deplanarized. While all conformers of **Bpy2** in the excited-state are planar, deplanarization can only arise from the statistical Si/Al distribution in the framework of zeolite L. Due to the distinct distribution around one **Bpy2** molecule, all molecule structures differ from each other and are more or less deplanarized. Nevertheless, after optimization, three "preferred" energy regions, and hence, absorption and emission maxima regions are formed. This is in good agreement with the results of the matrix rank analysis where three distinct contributing species were found.

Acknowledgment. This work was supported by the research grant GR 1229/6-1 of Deutsche Forschungsgemeinschaft. Furthermore, G.J.M. would like to thank the Deutsche Forschungsgemeinschaft for the Heisenberg Fellowship MO 1062/1-1 and for the research grant MO 1062/3-1.

References and Notes

(1) Friend, R. H. *Pure Appl. Chem.* **2002**, *73*, 430.
(2) Scherf, U. *Top. Curr. Chem.* **1999**, *201*, 163.
(3) Yamamoto, T.; Hayashida, N. *React. Funct. Polym.* **1998**, *37*, 1.
(4) Cacialli, F. *Phil. Trans. R. Soc. London, Ser. A* **2000**, *358*, 173.
(5) Kim, J. *Pure Appl. Chem.* **2002**, *74*, 2031.
(6) Saxena, V.; Malhotra, B. D. *Curr. Appl. Phys.* **2003**, *3*, 293.
(7) Armstrong, N. R.; Wightman, R. M.; Gross, E. M. *Ann. Rev. Phys. Chem.* **2001**, *52*, 391.
(8) *Electronic Materials: The Oligomer Approach*; Müllen, K., Wegner G. Eds.; Wiley-VCH: New York **1998**.
(9) Bredas, J.-L.; Beljonne, D.; Coropceanu, V.; Cornil, *J. Chem. Rev.* **2004**, *104*, 4971.
(10) Imamura, A., Hoffmann, R. *J. Am. Chem. Soc.* **1968**, *90*, 5379.
(11) Grummt, U.-W.; Birckner, E.; Klemm, E.; Egbe, D. A. M.; Heise, B. *J. Phys. Org. Chem.* **2000**, *13*, 112.
(12) Najbar, J. private communication.
(13) Shpol'skii, E. V.; Il'na, A. A.; Klimova, L. A.; *Dokl. Akad. Nauk SSSR* **1952**, *87*, 935.
(14) Calzaferri, G.; Brühwiler, D.; Megelski, S.; Pfenniger, M.; Pauchard, M.; Hennessy, B.; Maas, H.; Devaux, A.; Graf, U. *Solid State Sci.* **2000**, *2*, 421.
(15) Calzaferri, G.; Huber, S.; Maas, H.; Minkowski, C. *Angew. Chem.* **2003**, *113*, 3860.
(16) Megelski, S.; Calzaferri, G. *Adv. Funct. Mater.* **2001**, *11*, 277.
(17) Bärlocher, C.; Meier, W. M.; Olsen, D. H. *Atlas of Zeolite Framework Types*, 5th ed.; Elsevier:Amsterdam, 2001.
(18) Egbe, D. A. M.; Klemm, E. *Macromol. Chem. Phys.* **1998**, *199*, 2683.
(19) Nakatsuji, S.; Matsuda, K.; Uesugi, Y.; Nakashima, K.; Akiyama, S.; Fabian, W. J. *Chem. Soc., Perkin Trans.* **1992**, *1*, 755.
(20) Brunauer, S.; Deming, L. S.; Deming, W. S.; Teller, E. *J. Am. Chem. Soc.* **1940**, *62*, 1723.
(21) Brunauer, S.; Emmett, P. H.; Teller, E. *J. Am. Chem. Soc.* **1938**, *60*, 309.
(22) Ruiz, A. Z.; Brühwiler, D.; Ban, T.; Calzaferri, G. *Monatsh. Chem.* **2005**, *136*, 77.
(23) Ko, Y. S.; Ahn, W. S. *J. Ind. Eng. Chem.* **2004**, *10*, 636.
(24) Hirano, M.; Kato, M.; Asada, E.; Tsutsumi, K.; Shiraishi, A. *Adv. X-Ray Chem. Anal. Jpn.* **1992**, *23*, 101.
(25) Peintler, G.; Nagypál, I.; Iancsó, A.; Epstein, I. R.; Kustin, K. *J. Phys. Chem. A* **1997**, *101*, 8013.
(26) Frisch, M. J.; Trucks, G. W.; Schlegel, H. B.; Scuseria, G. E.; Robb, M. A.; Cheeseman, J. R.; Montgomery, J. A., Jr.; Vreven, T.; Kudin, K. N.; Burant, J. C.; Millam, J. M.; Iyengar, S. S.; Tomasi, J.; Barone, V.; Mennucci, B.; Cossi, M.; Scalmani, G.; Rega, N.; Petersson, G. A.; Nakatsuji, H.; Hada, M.; Ehara, M.; Toyota, K.; Fukuda, R.; Hasegawa, J.; Ishida, M.; Nakajima, T.; Honda, Y.; Kitao, O.; Nakai, H.; Klene, M.; Li, X.; Knox, J. E.; Hratchian, H. P.; Cross, J. B.; Bakken, V.; Adamo, C.; Jaramillo, J.; Gomperts, R.; Stratmann, R. E.; Yazyev, O.; Austin, A. J.; Cammi, R.; Pomelli, C.; Ochterski, J. W.; Ayala, P. Y.; Morokuma, K.; Voth, G. A.; Salvador, P.; Dannenberg, J. J.; Zakrzewski, V. G.; Dapprich, S.; Daniels, A. D.; Strain, M. C.; Farkas, O.; Malick, D. K.; Rabuck, A. D.; Raghavachari, K.; Foresman, J. B.; Ortiz, J. V.; Cui, Q.; Baboul, A. G.; Clifford, S.; Cioslowski, J.; Stefanov, B. B.; Liu, G.; Liashenko, A.; Piskorz, P.; Komaromi, I.; Martin, R. L.; Fox, D. J.; Keith, T.; Al-Laham, M. A.; Peng, C. Y.; Nanayakkara, A.; Challacombe, M.; Gill, P. M. W.; Johnson, B.; Chen, W.; Wong, M. W.; Gonzalez, C.; Pople, J. A. *Gaussian 03*, revision D.01; Gaussian, Inc.: Wallingford, CT, 2004.
(27) Merrit, L. L.; Schroeder, E. D. *Acta Cryst.* **1956**, *9*, 801.
(28) Nakamoto, K. J.; *Phys. Chem.* **1960**, *64*, 1420.
(29) Göller, A. H.; Grummt, U.-W. *Chem. Phys. Lett.* **2002**, *345*, 233.
(30) Grummt, U.-W.; Erhardt, S. *J. Mol. Structure (THEOCHEM)* **2004**, *685*, 133.
(31) Moisette, A.; Gener, I.; Brémard, C. *J. Phys. Chem. B* **2001**, *105*, 5647.
(32) Maseras, F.; Morokuma, K. *J. Comput. Chem.* **1995**, *16*, 1170.
(33) Vreven, T.; Morokuma, K. *J. Comput. Chem.* **2000**, *21*, 1419.
(34) Dapprich, S.; Komáromi, I.; Byun, K. S.; Morokuma, K. Frisch, M. J. *J. Mol. Struct. (THEOCHEM)* **1999**, *461*, 1.